Deletion of H-ferritin in macrophages alleviates obesity and diabetes induced by high-fat diet in mice

Yasumasa Ikeda[1*], Hiroaki Watanabe[1,2*], Tetsuya Shiuchi[3], Hirofumi Hamano[4], Yuya Horinouchi[1], Masaki Imanishi[4], Mitsuhiro Goda[4], Yoshito Zamami[2,4], Kenshi Takechi[5], Yuki Izawa-Ishizawa[6], Licht Miyamoto[7], Keisuke Ishizawa[2,4], Ken-ichi Aihara[8], Koichiro Tsuchiya[7], Toshiaki Tamaki[1,9]

[1]Department of Pharmacology, [2]Department of Clinical Pharmacology, [3]Department of Integrative Physiology, [7]Department of Medical Pharmacology, [8]Department of Community Medicine for Diabetes and Metabolic Disorders, Institute of Biomedical Sciences, Tokushima University Graduate School, Tokushima, Japan

Institute of Biomedical Sciences, Tokushima University Graduate School, Tokushima, Japan

[4]Department of Pharmacy, [5]Clinical Trial Center for Developmental Therapeutics, Tokushima University Hospital, Tokushima, Japan

[6]AWA support center, Tokushima University, Tokushima, Japan

[9]Anan Medical Center, Tokushima, Japan

*These authors contributed equally to this work.

Corresponding author: Yasumasa Ikeda, MD, PhD

Department of Pharmacology, Institute of Biomedical Sciences,

Tokushima University Graduate School,

3-18-15 Kuramoto-cho, Tokushima, 770-8503, Japan

E-mail: yasuike@tokushima-u.ac.jp

Tel: +81-88-633-7061, Fax: +81-88-633-7062

ORCID: https://orcid.org/0000-0003-4318-7349

Word counts: 3997

Abstract

Aims/hypothesis

Iron accumulation affects obesity and diabetes, both of which are ameliorated by iron reduction. Ferritin, an iron storage protein, plays a crucial role in iron metabolism. H-ferritin exerts its cytoprotective action by reducing toxicity via its ferroxidase activity. We investigated the role of macrophage H-ferritin in obesity and diabetes.

Methods

Conditional macrophage-specific H-ferritin knockout (LysM-Cre *Fth*KO) mice were used and divided into 4 groups; Wild-type (WT) and LysM-Cre *Fth*KO mice with normal diet (ND), and WT and LysM-Cre *Fth*-KO mice with high-fat diet (HFD).

Results

Iron concentration reduced, and mRNA expression of ferroportin increased in macrophages from LysM-Cre *Fth*KO mice. HFD-induced obesity was lower in LysM-Cre *Fth*KO mice than in WT mice at 12 weeks (body weight (g); KO 34.6 ± 5.6 vs. WT 40.1 ± 5.2). mRNA expression of inflammatory cytokines, infiltrated macrophages, and oxidative stress increased in the adipose tissue of WT mice with HFD, but was not elevated in LysM-Cre *Fth*KO mice with HFD. However, WT mice with

HFD had elevated iron concentration in adipose tissue and spleen, which was not observed in LysM-Cre *Fth*KO mice with HFD (adipose (μmol Fe/g protein); KO 1496 ± 479 vs. WT 2316 ± 866, spleen (μmol Fe/g protein); KO 218 ± 54 vs. WT 334 ± 83). Moreover, HFD administration impaired both glucose tolerance and insulin sensitivity in WT mice, which was ameliorated in LysM-Cre *Fth*KO mice. In addition, energy expenditure, mRNA expression of thermogenic genes, and body temperature were higher in KO mice with HFD than WT mice with HFD. In *vitro* experiments showed that iron content was reduced, and LPS-induced TNF-α mRNA upregulation was inhibited in a macrophage cell line transfected with *Fth* siRNA.

Conclusions/interpretation

Deletion of macrophage H-ferritin suppresses the inflammatory response by reducing intracellular iron levels, resulting in the prevention of HFD-induced obesity and diabetes. The findings from this study highlight macrophage iron levels as a potential therapeutic target for obesity and diabetes.

Keywords: diabetes, H-ferritin, inflammation, iron, macrophage, obesity

Abbreviations

HFD High-fat diet

FTH	Ferritin heavy chain (H-ferritin)
FTL	Ferritin light chain (L-ferritin)
FPN	Ferroportin
LysM	Lysozyme M

Research in context

What is already known about this subject?

• Increased body iron content is related to obesity and diabetes. Iron reduction ameliorates them. However, iron-deficient anaemia is induced due to non-specific iron reduction.

• Macrophages play a key role in the pathogenesis of obesity and diabetes through chronic inflammation.

• The pro-inflammatory M1 phenotype involves intracellular iron retention with the divergent expression of iron-related proteins and iron content in macrophages.

What is the key question?

• The reduction of macrophage iron content may ameliorate obesity and diabetes by the reduced inflammatory response.

What are the new findings?

• Conditional gene deletion of H-ferritin results in the reduction of iron content in macrophages and spleen without anaemia.

• High fat diet-induced obesity and diabetes were lower in macrophage-specific H-ferritin knockout mice.

• The knockout mice showed less inflammatory changes and oxidative stress in the adipose tissue.

How might this impact on clinical practice in the foreseeable future?

• Control of iron levels in macrophages is a potential therapeutic target for obesity and diabetes.

Introduction

Iron is an essential micromineral for all living beings. In contrast, excessive amount of iron induces oxidative stress by catalysing toxic hydroxy-radical production via the Fenton reaction. In hereditary iron overload disorders, cardiomyopathy, hepatic injury, and diabetes are caused by oxidative stress via ectopic tissue accumulation of excess iron [1]. Increased body iron content can be related to many diseases, including liver disease [2, 3], obesity [4], diabetes [5], cardiovascular disease [6, 7], and kidney disease[8]. Therefore, iron reduction is an effective strategy for ameliorating the pathological condition in such diseases, as shown by both clinical [9, 10] and experimental studies [11-14].

In terms of the dynamics of iron metabolism, iron is mostly recycled in the human body, since daily iron intake and excretion are only 1-1.5 mg each. Body iron is mostly located in erythrocytes (>70%) as haemoglobin. Macrophages phagocytosise senescent red blood cells (RBCs) and release iron obtained from haemoglobin into circulation, where it binds to plasma transferrin [15]. Thus, macrophages are central regulators of body iron homeostasis through the recycling of iron.

Macrophages undergo polarization to form either the pro-inflammatory phenotype (M1: classically activated) or the anti-inflammatory phenotype (M2: alternatively activated) [16]. These two phenotypes are characterized by divergent expression of iron-related proteins and iron content [17, 18]. M1 macrophages have increased iron content through the expression of high levels of the iron storage protein, H-ferritin (ferritin heavy chain; FTH) and low levels of the iron export protein ferroportin (FPN). In contrast, M2 macrophages have low iron content expression with low levels of H-ferritin and high levels of FPN. Differences in polarization between M1 and M2 may involve intracellular iron content, affecting macrophage function, especially in the aspect of proinflammatory change [19]. We found that FTH protein expression colocalizes with the increase in infiltrated macrophages in the adipose tissue of obese KKAy mice [11]. Additionally, increased iron content enhances the lipopolysaccharide (LPS)-induced inflammatory cytokine production in hepatic macrophages [20], and an iron chelator (deferoxamine) suppresses cytokine production in mouse bone marrow macrophages [21]. We hypothesized that the coordination of

ferritin and intracellular iron is a determining factor in the polarization of macrophages to the inflammatory phenotype.

In this study, we aimed to explore the role of macrophage FTH in obesity and diabetes induced by high-fat diet using macrophage-specific *Fth* knockout mice.

Methods

Materials

We purchased high-fat diet (HFD-60) and control diet (AIN-93M) from Oriental Yeast Co., Ltd. (Tokyo, Japan). The following commercially available antibodies were used: anti-ferritin heavy chain (FTH), anti-ferritin light chain (FTL), anti-$p22^{phox}$ (Santa Cruz Biotechnology, Inc., Dallas, TX), anti-phospho-SAPK/JNK (Thr183/Tyr185), anti-total SAPK/JNK, anti-phospho-p44/42 MAPK (Extracellular Signal-regulated Kinase 1/2 (ERK1/2)), anti-total p44/42 MAPK (ERK1/2) (Cell Signaling Technology, Danvers, MA), anti-F4/80 (Bio-Rad Laboratories, Inc. Tokyo, Japan), anti-4-hydroxynonenal (Japan Institute for the Control of Aging (JaICA), Nikken SEIL Co., Ltd., Shizuoka, Japan) and anti-α-tubulin (protein loading control, Merck KGaA, Darmstadt, Germany).

Animal preparation and procedures

Floxed *Fth* mice (C57BL/6J background) were purchased from Jackson Laboratory (Bar Harbor, Maine, USA). Lysozyme M (LysM)-Cre mice (C57BL/6J background) were gifted by Dr. Ken-ichi Aihara (Tokushima University). This cross generated mice carrying both the Cre gene and the heterozygous floxed *Fth* gene (LysM-Cre *Fth* fl/+). These mice were further mated with floxed *Fth* mice to generate LysM-Cre *Fth* knockout (KO) mice. Floxed *Fth* littermate mice without the LysM Cre gene were used as control wild-type (WT) mice. The male mice were randomly divided into the following four groups at six-weeks of age: WT mice with normal diet (ND), LysM-Cre *Fth* KO mice with ND, WT mice with high-fat diet (HFD), and LysM-Cre *Fth* KO mice with HFD. The mice were maintained with ad-libitum access to water and the corresponding diet. Twelve weeks later, the mice were euthanized by intraperitoneally injecting an overdose of anaesthesia, and tissues were removed and stored at −80°C until further use. All experimental procedures for mice were performed in accordance with the guidelines of the Animal Research Committee of Tokushima University Graduate School, and the protocol was approved by the Institutional Review

Board of Tokushima University Graduate School for animal protection (Permit Number: T28-49).

Peritoneal macrophage isolation

After anaesthesia, mice were intraperitoneally injected with 10 ml sterilized PBS. The abdomen was gently massaged for 5 min, and then phosphate-buffered saline (PBS) was recovered. Collected intraperitoneal PBS was centrifuged at 1.4×g incubated with RBC lysis buffer for 5 min, and washed and re-centrifuged with fresh PBS twice.

Extraction of tissues after insulin stimulation

After a 24-h fasting, mice under anaesthesia were injected with 1 U/kg insulin through the inferior vena cava. After 3 min, epididymal fat, liver, and gastrocnemius muscle were immediately removed and used for analysis.

Cell culture and small interference RNA transfection

The RAW264.7 mouse macrophage cells were purchased from DS Pharma Biomedical Co., Ltd. (Osaka, Japan), and were maintained and sub-cultured in DMEM containing 10% FBS, according to the culture protocol. siRNA targeting mouse *Fth* and a non-targeting siRNA control sequence were purchased from Dharmacon (a Horizon

Discovery Group Co., Cambridge, UK). Transfection of siRNA was performed as described previously [22]. Cells were used for further experiments after 48 h of transfection and then stimulated with 100 ng/ml LPS (FUJIFILM Wako Pure Chemical Corporation, Osaka, Japan) for 2 h.

RNA extraction and mRNA expression analysis

The methods used for RNA extraction, cDNA synthesis, and quantitative RT-PCR have been previously described [11]. Briefly, the tissues or cells were homogenized in RNAiso reagent (Takara Bio, Otsu, Japan). RNA extraction and cDNA synthesis were performed according to the manufacturer's instructions (PrimeScript RT reagent kit with gDNA Eraser (Perfect Real Time), Takara Bio). Quantitative RT-PCR was performed using the CFX Connect Real-Time PCR Detection System (Bio-Rad Laboratories, Hercules, CA, USA) with SYBR Green (THUNDERBIRD® SYBR® qPCR Mix, TOYOBO Co., Ltd., Osaka, Japan). The mRNA expression levels were normalized using 36B4 expression, and the values were compared to the control group in terms of relative fold change. The primer sets used are shown in table 1.

Protein extraction and western blot analysis

Protein preparation and western blotting were performed as previously described in detail [11]. The tissue or cell samples were homogenized or sonicated in a protein lysis buffer containing proteinase inhibitors and a phosphatase inhibitor. The extracted proteins were boiled for 5 min in Laemmli sample buffer and used for western blotting. The visualized immunoreactive protein bands were semi-quantified by densitometric analysis using Image J software (version 1.38, National Institutes of Health, Bethesda, MD, USA). The antibodies were used at the following dilutions: anti-FTH (1:250), anti-FTL (1:250), anti-phospho-JNK (1:1000), anti-total JNK (1:1000), anti-phospho-ERK1/2 (1:1000), anti-total ERK1/2 (1:1000), anti-phospho-Akt (1:500), anti-total Akt (1:1000), anti-phospho-IR β (1:1000), anti-total IR β (1:1000), anti-$p22^{phox}$ (1:250), and anti-tubulin (1:1000).

Histological analysis of adipocyte size

The epididymal fat tissue was fixed in 4% paraformaldehyde. After defatting and paraffin-embedding, the samples were cut into 3-μm-thick sections and stained with haematoxylin-eosin. Adipocyte size was determined by the average of ten random fields for each mouse [11].

Haematological analysis and blood chemistry

Whole blood cell counts were performed by Shikoku Chuken (Kagawa, Japan). Blood glucose levels and insulin levels were measured by using an ACCU-CHEK Aviva Kit (Roche Diagnostics, Basel, Switzerland) and a Mouse Insulin ELISA Kit (Morinaga Institute of Biological Science, Yokohama, Japan), respectively [11]. Plasma levels of TNF-α and adiponectin were determined using commercial ELISA kits (Quantikine ELISA Kit, R&D Systems, Minneapolis, MN, USA).

Glucose tolerance test

After fasting for 24 h, mice were intraperitoneally injected with 20% glucose solution (2.0 g/kg body weight). Blood was obtained from a tail vein at scheduled time points (0, 30, 60, and 120 min), and blood glucose levels were measured [11].

Insulin tolerance test

After a 4-h fasting, the mice were subjected to an insulin tolerance test. They were injected intraperitoneally with insulin (0.75 U/kg body weight; Humulin R; Eli Lilly, Indianapolis, IN). Blood glucose levels were measured at scheduled times (0, 15, 30, 60, and 120 min) [11].

Immunohistochemistry of macrophages in adipose tissues

Immunohistochemical staining of F4/80 was performed as described previously [11]. To evaluate macrophage infiltration, ten microscopic fields were randomly selected and F4/80 positive cells were counted.

Detection of oxidative stress in adipose tissue

Oxidative stress was evaluated by 4-hydroxynonenal (4-HNE) staining. In brief, paraffin sections were de-paraffinized and rehydrated, and then boiled with antigen retrieval 10 mM citrate buffer for 10 min and cooled for 20 min. After blocking, sections were incubated with 4-HNE antibody (1:50) at 4 °C overnight. Antibody distribution was visualized using immunofluorescence (Alexafluor; Life Technology, Tokyo, Japan). The sections incubated without primary antibody were used as negative controls.

Measurement of iron content

Tissue iron content was measured using an iron assay kit (Metallo assay LS, Metallogenics, Chiba, Japan) [12]. Iron concentration was corrected using protein concentration and expressed as μmol Fe per g protein concentration.

Metabolic measurement and body temperature

ARCO-2000 (ARCO SYSTEM Inc., Chiba, Japan) was used to measure oxygen consumption (VO_2) and respiratory quotient (RQ). Mice were placed in ACTIMO-100N (SHINFACTORY Co. Ltd., Fukuoka, Japan) with free access to food and water, allowing them to acclimatize in individual metabolic cages for 72 h before any measurements. The data were acquired at 12 h intervals for 24 h. A rectal probe (BP98A Softron Corp., Tokyo, Japan) measured the body temperature of mice.

Statistical analysis

Data are presented as mean ± standard deviation (mean ± SD). An unpaired, two-tailed, Student's *t*-test was used for comparison between the two groups. For comparison between more than two groups, the statistical significance of each difference was evaluated using a post-hoc test (either Dunnett's method or Tukey–Kramer's method). Statistical significance was set at $P < 0.05$.

Results

Characteristics of LysM-Cre FthKO mice and WT mice

First, we examined the *Fth* deletion in macrophages and other tissues. As shown in Fig.1a, *Fth* mRNA was deleted in peritoneal macrophages and was reduced by half in liver samples. There was no difference detected in *Fth* mRNA expression in the heart, liver, spleen, kidney, adipose, and skeletal muscles between WT and KO mice. In terms of ferritin protein, FTH protein expression was reduced in macrophages and spleen, but not in the liver of LysM-Cre *Fth*KO mice, and there was no difference in FTL protein expression in macrophages, liver, and spleen between WT and KO mice (Fig.1b-d).

Iron concentration and iron-related gene expression in macrophages

In peritoneal macrophages, the iron concentration was lower in LysM-Cre *Fth*KO mice than in WT mice (Fig.1e). *FPN* and *HO-1* mRNA expression increased, whereas *TfR* mRNA expression showed a decrease in macrophages in LysM-Cre *Fth*KO mice (Fig.1f-h). These results suggest that the *Fth* gene deletion leads to the reduced intracellular iron concentration through the decrease in iron importer and the increase in iron exporter in macrophages.

Macrophage Fth deletion on body weight and adipose tissues

Next, we tested the role of the macrophage *Fth* gene on HFD-induced obesity and diabetes. No difference was seen in body weight (BW) gained during the experimental course between WT mice and KO mice. The BW of WT mice fed on HFD diet increased after 2 weeks, whereas it was suppressed in LysM-Cre *Fth*KO mice (Fig.2a and b). There was no difference in the daily calorie intake between WT mice and KO mice in the HFD-fed group (Fig.2c). The HFD-induced weight gain of adipose tissue was attenuated in KO mice compared to WT mice (Fig.2d-g). In histological analysis, HFD enlarged adipocyte size in epididymal fat, which was smaller in LysM-Cre *Fth*KO mice than in WT mice (Fig.2h and i). The distribution of adipocyte size indicated that LysM-Cre *Fth*KO mice with HFD increased the proportion of small-sized adipocytes and decreased the proportion of large-sized adipocytes (Fig.2j). Additionally, red blood cells, haemoglobin, and haematocrit were elevated in HFD-fed mice, and there was no difference in these parameters between WT mice and LysM-Cre *Fth*KO mice regardless of ND or HFD (Table 1).

Macrophage infiltration and inflammatory cytokine expression in adipose tissue

As shown in Fig.3a and b, the number of F4/80-positive cells was increased in epididymal fat of HFD-fed WT mice, and it was significantly inhibited in HFD-fed KO mice. Similar to the results of immunohistochemical analysis, mRNA expression of *F4/80*, *CD68* was increased in epididymal fat of HFD-fed WT mice, and they were significantly inhibited in HFD-fed KO mice (Fig.3c and d). The mRNA expression of inflammatory cytokines such as *Tnf-α*, *Mcp-1*, *Il-1ß*, and *Il-6*, were upregulated in epididymal fat of WT mice with HFD, but were diminished in KO mice with HFD (Fig.3f-i). *Adiponectin* mRNA expression was reduced, and *Leptin* mRNA expression was increased in the fat of HFD-fed WT mice, while these changes were ameliorated in HFD-fed KO mice (Fig.3j and k). Additionally, mRNA expression of *CD11c*, a surface marker of M1-like cells, was elevated in HFD-fed WT mice, but inhibited in HFD-fed KO mice (Fig.3e). In plasma, the HFD-induced increase in the TNF-α levels and decrease in adiponectin levels were also ameliorated in KO mice (Fig.3l and m). These results suggested that macrophage *Fth* deletion leads to inhibition of HFD-induced inflammation and the disorder of adipocytokines in fat.

Effect of macrophages Fth deletion on mitogen-activated protein kinase pathway and oxidative stress

Moreover, JNK and ERK1/2, members of the mitogen-activated protein kinase (MAPK) family, play an important role in inflammatory gene regulation [23]. Administration of HFD increased the phosphorylated levels of JNK, but not ERK1/2, in the fat of WT mice, and it was reduced in KO mice (Fig.4a-c). In adipose tissue, 4-HNE intensity was augmented in WT mice with HFD, and it was suppressed in HFD-fed KO mice (Fig.4d and e). NADPH oxidase is a source of reactive oxygen species, and increase in $p22^{phox}$ protein, a NADPH oxidase subunit with heme protein, was suppressed by iron reduction in obese adipose tissue [11]. Furthermore, $p22^{phox}$ was elevated in adipose tissue of WT mice with HFD, and it was suppressed in adipose tissue of KO mice with HFD (Fig.4f and g). Thus, HFD-induced inflammatory pathway activation and oxidative stress were inhibited in the fat of LysM-*Fth*KO mice.

Iron content in fat, spleen, and macrophages

In epididymal fat and spleen, tissue iron content was elevated in HFD-fed WT mice, and it was inhibited in HFD-KO mice (Fig.4h and i). Iron content in macrophages

was lower in KO mice than in WT mice. However, macrophage iron levels did not change by HFD in WT and KO mice (Fig.4j).

Macrophage Fth deletion on glucose tolerance, insulin sensitivity, and insulin signalling pathway

To examine whether macrophage *Fth* deletion affected glucose tolerance and insulin sensitivity, we subjected mice to intraperitoneally glucose tolerance tests and insulin tolerance tests, respectively. There was no difference in blood glucose levels between WT mice and KO mice with ND fed groups after glucose injection, and the degree of increase in blood glucose level after glucose injection was lower in HFD-fed KO mice than in HFD-fed WT mice (Fig. 5a and b). With IPITT, the reduction in the blood glucose levels was more in KO mice than in WT mice in HFD-fed groups, and there was no difference in blood glucose levels between WT mice and KO mice with ND-fed groups after insulin injection (Fig. 5c and d). The phosphorylation of the IRβ-Akt signalling pathway was increased in epididymal fat in ND-fed groups of both WT mice and KO mice after insulin stimulation. The phosphorylated levels of IRβ-Akt signalling after insulin stimulation was diminished in HFD-fed WT mice, and it was

ameliorated in the fat of HFD-fed KO mice (Fig. 5e and f). In the liver and skeletal muscle, the reduced phosphorylation of IRβ-Akt signalling after insulin stimulation was also ameliorated in HFD-fed KO mice (Fig. 6a-f). The mRNA expression of inflammatory cytokines (except for *Il-6*) was increased in HFD-fed WT mice, which was diminished in HFD-fed KO mice (Fig. 6g-n). The fasting plasma glucose level was significantly higher in HFD-fed WT mice than in HFD-fed KO mice. The plasma insulin level was markedly elevated in HFD-fed WT mice, and it was significantly lower in HFD-fed KO mice (Table 1). These results suggest that macrophage *Fth* deletion leads to the reduction in glucose tolerance and insulin resistance both through inhibiting inflammation and maintaining insulin signalling in fat, liver, and skeletal muscle under obesity and diabetes.

Effect of Macrophage Fth deletion on energy expenditure in mice with HFD

We further analysed the energy expenditure. The oxygen consumption (VO_2) and energy expenditure were significantly higher in HFD-fed KO mice during the dark phase, while RQ was lower in HFD-fed KO mice compared to HFD-fed WT mice during the dark and total phase (Fig. 7a-c). Additionally, the body temperature and

several thermogenic gene expressions (*UCP-3*, *Adrb3*, *Pparg1a*, *Dio2*, and *Prdm16*) were significantly higher in the fat of KO mice with HFD compared to the WT mice with HFD (Fig. 7d-k). These results partly contributed to the decreased body-weight gain in HFD-fed KO mice.

Effect of Fth deletion on LPS-induced inflammation in vitro experiments

We examined the effect of *Fth* deletion by using RAW264.7 cells derived from mice peritoneal macrophages. siRNA of *Fth* gene transduction reduced *Fth* mRNA by approximately 20 % and mimicked the phenotype of iron-related genes and iron content in macrophages of LysM-Cre *Fth*KO mice (Fig. 8a-e). LPS stimulation increased TNF-α mRNA expression, and it was partly inhibited with *Fth* siRNA transduction (Fig. 8f).

Discussion

Deletion of macrophage *Fth* gene reduced intracellular iron content via changes in iron transporter expression, and it inhibited the LPS-induced inflammatory response. Macrophage *Fth* gene KO mice showed diminished HFD-induced

inflammatory changes and macrophage infiltration in adipose tissue, contributing to the suppression of obesity and diabetes.

Ferritin is a ubiquitous iron-binding protein and the main form of intracellular iron storage. It is composed of 24-mer heteromultimers of 2 subtypes: H (FTH) and L (FTL) subunits [24]. FTH has ferroxidase activity (converts Fe^{2+} to Fe^{3+}). Meanwhile, FTL takes up and maintains iron content by nucleation, although it lacks ferroxidase activity [25-27]. Ferritin synthase is mainly regulated by iron at the translational level through both iron-regulatory proteins and iron-responsive elements in the 5'-untranslated regions of *Fth* and *Ftl* RNAs [28], and in an iron-independent manner including oxidative stress [29], and in the presence of inflammatory cytokines [30, 31]. In addition to being an iron-storage protein, FTH is normally thought to exert a cytoprotective effect by its anti-oxidant property that inhibits Fenton reaction via its ferroxidase activity and nucleation for free iron ions [26, 27]. Indeed, several studies have shown the protective action of FTH on heart failure (cardiomyocyte) [32], acute kidney injury (proximal tubule) [33], and ischemic liver injury (hepatocyte) [34]. In contrast, myeloid (macrophage) *Fth* gene deficiency alleviates unilateral ureter

obstruction-induced renal fibrosis in mice, although the mechanism has not been described in detail [35]. Thus, FTH function might vary depending on cells and tissues, and macrophage *Fth* deletion exerts a favourable effect on at least renal fibrosis, obesity, and diabetes.

Whole-body iron reduction by an iron chelator or an iron-restricted diet has been shown to be beneficial for the inhibition of inflammatory cytokines and oxidative stress in rat and mice models of obesity and type 2 diabetes [11, 36, 37] However, these advantages are counterbalanced by iron-deficient anaemia. In this study, macrophage deletion of the *Fth* gene resulted in reduced iron content, contributing to the inhibitory effect of HFD-induced obesity and diabetes with the reduction of inflammatory cytokines, macrophage infiltration, and oxidative stress without presenting anaemia. HFD-induced increase of pro-inflammatory cytokine expression (M1-like markers; IL-1β, TNF-α, CD68) was diminished in the fat of KO mice compared to WT mice. Similarly, LPS-induced increase of TNF-α expression was also alleviated in RAW264.7 macrophage cells transfected with *Fth* siRNA. These findings suggest that macrophage iron plays a pivotal role in the development of obesity and diabetes, and

macrophage-specific reduction of iron may be a target for metabolic disorders through the inhibition of the inflammatory response.

It is well-established that chronic low-grade inflammation is linked to the development of insulin resistance, obesity, and diabetes [38]. An increase of infiltrated macrophages is seen in visceral fat of obese subjects, and body weight loss leads to a reduction of inflammatory markers and infiltrated macrophages [39, 40]. Diet-induced obesity promotes macrophages to switch to the M1 pro-inflammatory phenotype from M2 anti-inflammatory phenotype, contributing to insulin resistance [41]. A shift in the polarization of adipose tissue macrophages to a proinflammatory phenotype plays a crucial role in the development of obesity and diabetes. Deletion of *the Fth* gene altered the expression of iron-related genes (decrease of *TfR* expression and the increase of *FPN* and *HO-1* expression) in addition to iron content reduction. Iron metabolism is suggested to involve the regulation of macrophage polarization. M1-polarized proinflammatory macrophages increase intracellular iron retention with reduction of TfR and FPN and elevation of FTH, while, M2-polarized anti-inflammatory macrophages decrease intracellular iron content with elevation of TfR and FPN and

reduction of FTH *in vitro* [18]. In *in vivo* lean adipose tissue, all infiltrated macrophages with low or high iron are of the M2-like phenotype with greater expression of M2 genes and a reduction in the expression of M1 genes, suggesting the promotion of iron recycling. In obesity, macrophages with high iron levels become more inflammatory and lose the property of iron handling, indicating changes in their polarization and phenotype [42]. In this study, *Fth* gene deletion inhibited proinflammatory response induced by HFD or LPS. However, the change of *TfR* expression, not *FPN* and *Hmox1*, was in disagreement with that of the M2-like phenotype. However, the effect of H-ferritin overexpression is controversial. H-ferritin overexpression itself increases iNOS expression [35], while ferritin induction alleviates LPS-induced inflammatory response [43]. Further investigation is necessary for clarifying the role of FTH on macrophages in detail.

We showed that LysM-Cre *Fth*KO mice had higher energy expenditure compared to WT mice in HFD administration. The body temperature and expression of thermogenic genes in epididymal fat were also higher in HFD-fed KO mice compared to the HFD-fed WT mice. White-to-brown fat transition (known as beige adipocyte)

plays a significant role in regulating body weight and protecting against diabetes and obesity through thermogenesis [44]. Therefore, the promotion of browning of white fat may partly involve the alleviation of HFD-induced-obesity and diabetes in LysM-Cre *Fth*KO mice.

In terms of tissue iron content, the HFD induced an increase of tissue iron concentration in epididymal fat and spleen in WT mice, but suppressed tissue iron concentration in LysM-Cre *Fth*KO mice. However, iron content was not increased by HFD in isolated peritoneal macrophages, although macrophage iron content remained lower in KO mice than in WT mice with ND or HFD. Increased iron content in fat and spleen might be due to the increase in infiltrated macrophages that supply iron to local tissues in mice with HFD. In *in vitro* models, M1 macrophages display an iron sequestration phenotype with an associated increase in FTH expression. Similar results were obtained in mouse models where the iron content of macrophage with both subtypes was not increased by HFD administration, although the iron content was increased in HFD-induced hypertrophied adipocytes [42]. Thus, there is the discrepancy of M1 macrophage iron content between the in vitro model and in vivo model. In

contrast, macrophage iron release is necessary for the repair of skeletal muscle injury through myogenic differentiation. There are no differences in macrophage iron content during muscle injury [45], suggesting macrophages as the suppliers of iron to local tissue without themselves exhibiting any change in iron content due to rapid iron release. Further studies are needed to clarify the accurate mechanism.

Body iron content is normally lower in females than males, and several studies have shown the effect of sex hormones on iron metabolism [22, 46]. A limitation of this study is that we only used male mice. Therefore, further study is necessary for clarifying the effect of *Fth* deletion on macrophages in both the genders.

In conclusion, deletion of the *Fth* gene in macrophages leads to a reduction of both intracellular iron concentration and inflammatory response, resulting in the prevention of HFD-induced obesity and diabetes. Control of macrophage-specific iron levels is, thus, a potential therapeutic target for regulating chronic inflammation.

Acknowledgments

We appreciate the excellent technical advice by the Support Centre for Advanced Medical Sciences, Institute of Biomedical Sciences, Tokushima University Graduate School. We would like to thank Editage (www.editage.jp) for their help with English language editing.

Funding

This work was supported by the Japan Society for the Promotion of Science (JSPS) KAKENHI Grant (18K08480 to Y.I).

Duality of interest

The authors declare that there is no duality of interest associated with this manuscript.

Author Contributions

Y.I. conceived the study, designed experiments, acquired and analysed the data, wrote the manuscript. H.W., T.S., and H.H. acquired and analysed the data. Y.H. contributed to the analysis and interpretation of the data and reviewed the manuscript. M.I., M.G., Y.Z., K.T., Y.I-I., L.M., K.I., K-i.A., K.T., and T.T. contributed to the analysis and interpretation of the data. Y.I. is the guarantor of this work and, as such, had full access to all the data in the study and takes responsibility for the integrity of the data and the

accuracy of the data analysis. All the authors approved the final version of this manuscript.

References

[1] Camaschella C (2005) Understanding iron homeostasis through genetic analysis of hemochromatosis and related disorders. Blood 106(12): 3710-3717. 2005-05-1857 [pii]

10.1182/blood-2005-05-1857

[2] Ryan Caballes F, Sendi H, Bonkovsky HL (2012) Hepatitis C, porphyria cutanea tarda and liver iron: an update. Liver Int 32(6): 880-893. 10.1111/j.1478-3231.2012.02794.x

[3] Dongiovanni P, Fracanzani AL, Fargion S, Valenti L (2011) Iron in fatty liver and in the metabolic syndrome: a promising therapeutic target. J Hepatol 55(4): 920-932. 10.1016/j.jhep.2011.05.008

[4] Nikonorov AA, Skalnaya MG, Tinkov AA, Skalny AV (2015) Mutual interaction between iron homeostasis and obesity pathogenesis. J Trace Elem Med Biol 30: 207-214. 10.1016/j.jtemb.2014.05.005

[5] Fernandez-Real JM, Manco M (2014) Effects of iron overload on chronic metabolic diseases. Lancet Diabetes Endocrinol 2(6): 513-526. 10.1016/S2213-8587(13)70174-8

[6] Kremastinos DT, Farmakis D (2011) Iron overload cardiomyopathy in clinical practice. Circulation 124(20): 2253-2263. 10.1161/CIRCULATIONAHA.111.050773

[7] Depalma RG, Hayes VW, Chow BK, Shamayeva G, May PE, Zacharski LR (2010) Ferritin levels, inflammatory biomarkers, and mortality in peripheral arterial disease: a substudy of the Iron (Fe) and Atherosclerosis Study (FeAST) Trial. J Vasc Surg 51(6): 1498-1503. 10.1016/j.jvs.2009.12.068

[8] Ribeiro S, Belo L, Reis F, Santos-Silva A (2016) Iron therapy in chronic kidney disease: Recent changes, benefits and risks. Blood Rev 30(1): 65-72. 10.1016/j.blre.2015.07.006

[9] Nakanishi T, Kuragano T, Nanami M, Otaki Y, Nonoguchi H, Hasuike Y (2010) Importance of ferritin for optimizing anemia therapy in chronic kidney disease. American journal of nephrology 32(5): 439-446. 10.1159/000320733

[10] Beaton MD, Chakrabarti S, Levstik M, Speechley M, Marotta P, Adams P (2013) Phase II clinical trial of phlebotomy for non-alcoholic fatty liver disease. Aliment Pharmacol Ther 37(7): 720-729. 10.1111/apt.12255

[11] Tajima S, Ikeda Y, Sawada K, et al. (2012) Iron reduction by deferoxamine leads to amelioration of adiposity via the regulation of oxidative stress and inflammation in obese and type 2 diabetes KKAy mice. Am J Physiol Endocrinol Metab 302(1): E77-86. ajpendo.00033.2011 [pii]

10.1152/ajpendo.00033.2011

[12] Ikeda Y, Enomoto H, Tajima S, et al. (2013) Dietary iron restriction inhibits progression of diabetic nephropathy in db/db mice. American journal of physiology Renal physiology 304(7): F1028-1036. 10.1152/ajprenal.00473.2012

[13] Ikeda Y, Horinouchi Y, Hamano H, et al. (2017) Dietary iron restriction alleviates renal tubulointerstitial injury induced by protein overload in mice. Sci Rep 7(1): 10621. 10.1038/s41598-017-11089-0

[14] Naito Y, Hirotani S, Sawada H, Akahori H, Tsujino T, Masuyama T (2011) Dietary iron restriction prevents hypertensive cardiovascular remodeling in dahl salt-sensitive rats. Hypertension 57(3): 497-504. HYPERTENSIONAHA.110.159681 [pii]

10.1161/HYPERTENSIONAHA.110.159681

[15] Ganz T (2012) Macrophages and systemic iron homeostasis. J Innate Immun 4(5-6): 446-453. 10.1159/000336423

[16] Mills CD, Kincaid K, Alt JM, Heilman MJ, Hill AM (2000) M-1/M-2 macrophages and the Th1/Th2 paradigm. J Immunol 164(12): 6166-6173

[17] Recalcati S, Locati M, Marini A, et al. (2010) Differential regulation of iron homeostasis during human macrophage polarized activation. Eur J Immunol 40(3): 824-835. 10.1002/eji.200939889

[18] Corna G, Campana L, Pignatti E, et al. (2010) Polarization dictates iron handling by inflammatory and alternatively activated macrophages. Haematologica 95(11): 1814-1822. 10.3324/haematol.2010.023879

[19] Recalcati S, Locati M, Gammella E, Invernizzi P, Cairo G (2012) Iron levels in polarized macrophages: regulation of immunity and autoimmunity. Autoimmun Rev 11(12): 883-889. 10.1016/j.autrev.2012.03.003

[20] Tsukamoto H, Lin M, Ohata M, Giulivi C, French SW, Brittenham G (1999) Iron primes hepatic macrophages for NF-kappaB activation in alcoholic liver injury. Am J Physiol 277(6): G1240-1250. 10.1152/ajpgi.1999.277.6.G1240

[21] Autenrieth IB, Bohn E, Ewald JH, Heesemann J (1995) Deferoxamine B but not deferoxamine G1 inhibits cytokine production in murine bone marrow macrophages. J Infect Dis 172(2): 490-496

[22] Ikeda Y, Tajima S, Izawa-Ishizawa Y, et al. (2012) Estrogen Regulates Hepcidin Expression via GPR30-BMP6-Dependent Signaling in Hepatocytes. PLoS One 7(7): e40465. 10.1371/journal.pone.0040465

PONE-D-12-05434 [pii]

[23] Li DQ, Luo L, Chen Z, Kim HS, Song XJ, Pflugfelder SC (2006) JNK and ERK MAP kinases mediate induction of IL-1beta, TNF-alpha and IL-8 following hyperosmolar stress in human limbal epithelial cells. Experimental eye research 82(4): 588-596. 10.1016/j.exer.2005.08.019

[24] Harrison PM, Arosio P (1996) The ferritins: molecular properties, iron storage function and cellular regulation. Biochimica et biophysica acta 1275(3): 161-203

[25] Lawson DM, Artymiuk PJ, Yewdall SJ, et al. (1991) Solving the structure of human H ferritin by genetically engineering intermolecular crystal contacts. Nature 349(6309): 541-544. 10.1038/349541a0

[26] Lawson DM, Treffry A, Artymiuk PJ, et al. (1989) Identification of the ferroxidase centre in ferritin. FEBS letters 254(1-2): 207-210

[27] Santambrogio P, Levi S, Cozzi A, Corsi B, Arosio P (1996) Evidence that the specificity of iron incorporation into homopolymers of human ferritin L- and H-chains is conferred by the nucleation and ferroxidase centres. The Biochemical journal 314 (Pt 1): 139-144

[28] Klausner RD, Harford JB (1989) cis-trans models for post-transcriptional gene regulation. Science 246(4932): 870-872

[29] Tsuji Y, Ayaki H, Whitman SP, Morrow CS, Torti SV, Torti FM (2000) Coordinate transcriptional and translational regulation of ferritin in response to oxidative stress. Molecular and cellular biology 20(16): 5818-5827

[30] Miller LL, Miller SC, Torti SV, Tsuji Y, Torti FM (1991) Iron-independent induction of ferritin H chain by tumor necrosis factor. Proceedings of the National Academy of Sciences of the United States of America 88(11): 4946-4950

[31] Rogers JT (1996) Ferritin translation by interleukin-1and interleukin-6: the role of sequences upstream of the start codons of the heavy and light subunit genes. Blood 87(6): 2525-2537

[32] Omiya S, Hikoso S, Imanishi Y, et al. (2009) Downregulation of ferritin heavy chain increases labile iron pool, oxidative stress and cell death in cardiomyocytes. J Mol Cell Cardiol 46(1): 59-66. 10.1016/j.yjmcc.2008.09.714

[33] Zarjou A, Bolisetty S, Joseph R, et al. (2013) Proximal tubule H-ferritin mediates iron trafficking in acute kidney injury. J Clin Invest 123(10): 4423-4434. 10.1172/JCI67867

[34] Berberat PO, Katori M, Kaczmarek E, et al. (2003) Heavy chain ferritin acts as an antiapoptotic gene that protects livers from ischemia reperfusion injury. FASEB J 17(12): 1724-1726. 10.1096/fj.03-0229fje

[35] Bolisetty S, Zarjou A, Hull TD, et al. (2015) Macrophage and epithelial cell H-ferritin expression regulates renal inflammation. Kidney Int 88(1): 95-108. 10.1038/ki.2015.102

[36] Minamiyama Y, Takemura S, Kodai S, et al. (2010) Iron restriction improves type 2 diabetes mellitus in Otsuka Long-Evans Tokushima fatty rats. Am J Physiol Endocrinol Metab 298(6): E1140-1149. ajpendo.00620.2009 [pii]

10.1152/ajpendo.00620.2009

[37] Yan HF, Liu ZY, Guan ZA, Guo C (2018) Deferoxamine ameliorates adipocyte dysfunction by modulating iron metabolism in ob/ob mice. Endocr Connect 7(4): 604-616. 10.1530/EC-18-0054

[38] Dandona P, Aljada A, Bandyopadhyay A (2004) Inflammation: the link between insulin resistance, obesity and diabetes. Trends Immunol 25(1): 4-7

[39] Cancello R, Henegar C, Viguerie N, et al. (2005) Reduction of macrophage infiltration and chemoattractant gene expression changes in white adipose tissue of morbidly obese subjects after surgery-induced weight loss. Diabetes 54(8): 2277-2286

[40] Cancello R, Tordjman J, Poitou C, et al. (2006) Increased infiltration of macrophages in omental adipose tissue is associated with marked hepatic lesions in morbid human obesity. Diabetes 55(6): 1554-1561. 10.2337/db06-0133

[41] Lumeng CN, Bodzin JL, Saltiel AR (2007) Obesity induces a phenotypic switch in adipose tissue macrophage polarization. J Clin Invest 117(1): 175-184. 10.1172/JCI29881

[42] Orr JS, Kennedy A, Anderson-Baucum EK, et al. (2014) Obesity alters adipose tissue macrophage iron content and tissue iron distribution. Diabetes 63(2): 421-432. 10.2337/db13-0213

[43] Zarjou A, Black LM, McCullough KR, et al. (2019) Ferritin Light Chain Confers Protection Against Sepsis-Induced Inflammation and Organ Injury. Front Immunol 10: 131. 10.3389/fimmu.2019.00131

[44] Wu J, Bostrom P, Sparks LM, et al. (2012) Beige adipocytes are a distinct type of thermogenic fat cell in mouse and human. Cell 150(2): 366-376. 10.1016/j.cell.2012.05.016

[45] Corna G, Caserta I, Monno A, et al. (2016) The Repair of Skeletal Muscle Requires Iron Recycling through Macrophage Ferroportin. J Immunol 197(5): 1914-1925. 10.4049/jimmunol.1501417

[46] Guo W, Bachman E, Li M, et al. (2013) Testosterone administration inhibits hepcidin transcription and is associated with increased iron incorporation into red blood cells. Aging Cell 12(2): 280-291. 10.1111/acel.12052

Figure legends

Figure 1. The differences of ferritin expression in various tissue between WT mice and LysM-*Fth* KO mice. (a) H-ferritin (*Fth*) mRNA expression in macrophage, heaty, liver, kidney, fat, and skeletal muscle. Values are expressed as mean ± SD. **P* < 0.05, ***P* < 0.01; n = 3-7 in each group. FTH and L-ferritin (FTL) protein expression in macrophage (b), spleen (c), and liver (d). Values are expressed as mean ± SD. **P* < 0.05, ***P* < 0.01; n = 4 in each group. (e) Iron content in macrophage. Values are expressed as mean ± SD. **P* < 0.05, ***P* < 0.01; n = 6-10 in each group. mRNA expression of *Fpn* (f), *Homx1* (g), and *Tfr* (h) in macrophage. Values are expressed as mean ± SD. ***P* < 0.01; n = 4-7 in each group. There was no significant difference in *Tfr* mRNA between WT and KO (p=0.08).

Figure 2. Body weight, fat weight and adipocyte size and distribution. (a) Changes in body weight in WT mice and LysM-*fth* KO mice with ND or HFD. Values are expressed as mean ± SD. **P* < 0.05, ***P* < 0.01 vs LysM-*fth* KO mice with HFD; n = 9-11 in each group. (b) Body weight at 12 weeks on diet. Values are expressed as mean ± SD. **P* < 0.05, ***P* < 0.01; n = 9-11 in each group. (c) Daily calorie intake. Values are expressed as mean ± SD. **P* < 0.05, ***P* < 0.01; n = 6-7 in each group.

Weight of epididymal fat (d), mesenteric fat (e), retroperitoneal fat (f), and subcutaneous fat (g) at 12 weeks on diet. Values are expressed as mean ± SD. *P < 0.05, **P < 0.01; n = 9-11 in each group. (h) Representative findings with haematoxylin-eosin staining of adipocytes in epididymal fat. Mean adipocyte size (i) and distribution of adipocyte sizes (j). Values are expressed as mean ± SD. n = 8.

Fig.3. Effect of macrophage *Fth* deletion on HFD-induced macrophage infiltration and inflammatory cytokines expression in adipose tissue. (a) Representative findings of immunohistochemical staining for infiltrated macrophages by F4/80 antibody (black arrows) in epididymal fat. (b) Semiquantitative analysis of the F4/80-positive cell. Values are expressed as mean ± SD. **P < 0.01; n = 8. Quantification of *F4/80* (c), *CD68* (d), and *CD11c* (e) mRNA in the fat of mice in each group. Values are expressed as mean ± SD. *P<0.05, **P<0.01, n=12 in each group. Quantitative analysis of mRNA expression for inflammatory cytokines (*Tnf-α* (f), *Mcp-1* (g), *Il-1β* (h), *Il-6* (i)), and adipokines (*adiponectin* (j), *Leptin* (k)) in the fat of mice in each group. Values are expressed as mean ± SD. *P < 0.05, **P < 0.01, n = 12 in each

group. Plasma concentration of TNF-α (l) and adiponectin (m). Values are expressed as mean ± SD. *P < 0.05, **P < 0.01, n = 12 in each group.

Fig. 4. Effect of macrophage Fth deletion on JNK and ERK signalling pathway. (a) Representative protein bands of phosphorylated JNK, total JNK, phosphorylated ERK1/2, total ERK1/2, and tubulin in epididymal fat of each mice. (b) Semi-quantitative analysis of densitometry for JNK and ERK1/2 phosphorylation. Values are expressed as mean ± SD. *P < 0.05, **P < 0.01, n = 8 in each group. Lipid peroxidation in epididymal adipose tissue. (d) Representative findings of immunohistochemistry for 4-hydroxynonenal. (e) Semiquantitative analysis of 4-Hydroxynonenal-positive intensity. Values are expressed as mean ± SD. *$P < 0.05$; n = 4. mRNA and protein expression of p22 ^{phox} in epididymal fat. (f) quantitative analysis of p22^{phox} mRNA expression. Values are expressed as mean ± SD. *$P < 0.05$, **P < 0.01, n = 8. (g) Representative images and semi-quantitative analysis of p22^{phox} protein expression. Values are expressed as mean ± SD. *$P < 0.05$, **P < 0.01, n = 4. Measurement of iron concentration in (h) Epididymal fat, (i) spleen, and (j) peritoneal

macrophage of each mice. Values are expressed as mean ± SD. *P < 0.05, **P < 0.01, n = 8-20 in each group.

Fig. 5. Deletion of macrophage *Fth* on glucose tolerance and insulin sensitivity in mice. (a) Changes in blood glucose level during intraperitoneal glucose tolerance test (IPGTT) in WT mice and LysM-*fth* KO mice with ND and HFD. Values are expressed as mean ± SD. *P < 0.05, n = 8-11 in each group. (b) Area under the curve of blood glucose level during IPGTT. Values are expressed as mean ± SD. *P < 0.05, n = 8-11 in each group. (c) Changes in blood glucose level during intraperitoneal insulin tolerance test (IPITT) in WT mice and LysM-*fth* KO mice on ND and HFD. Values are expressed as mean ± SD. *P < 0.05 , **P < 0.01, n = 8-14 in each group. (d) Area under the curve of blood glucose level during IPGTT. Values are expressed as mean ± SD. *P < 0.05, n = 8-14 in each group. Effect of macrophage *Fth* deletion on HFD-induced insulin resistance in epididymal fat. (e) Representative protein bands of phosphorylated IR β, total IR β, phosphorylated Akt, total Akt, and tubulin. Semi-quantitative analysis of densitometry for IR β (f) and Akt (g) phosphorylation in

fat tissue. Values are expressed as mean ± SD. *P < 0.05, **P < 0.01, n = 8-14 in each group.

Fig.6 Deletion of macrophage *Fth* on insulin sensitivity and inflammatory cytokines in liver and skeletal muscle of mice. (a) Representative protein bands of phosphorylated IR β, total IR β, phosphorylated Akt, total Akt, and tubulin. Semi-quantitative analysis of densitometry for IR β (b) and Akt (c) phosphorylation in the liver. Values are expressed as mean ± SD. *P < 0.05, **P < 0.01, n = 8 in each group. (d) Representative protein bands of phosphorylated IR β, total IR β, phosphorylated Akt, total Akt, and tubulin. Semi-quantitative analysis of densitometry for IR β (e) and Akt (f) phosphorylation in skeletal muscle Values are expressed as mean ± SD. *P < 0.05, **P < 0.01, n = 8 in each group. Quantitative analysis of mRNA expression for inflammatory cytokines in the liver (*Tnf-α* (g), *Mcp-1* (h), *Il-1β* (i), *Il-6* (j)) and gastrocnemius muscle (*Tnf-α* (k), *Mcp-1* (l), *Il-1β* (m), *Il-6* (n)). Values are expressed as mean ± SD. *P < 0.05, **P < 0.01, n = 10-12 in each group.

Fig.7. Deletion of macrophage *Fth* on metabolic expenditure and thermogenesis in mice with HFD. (a) Effect of macrophage *Fth* deletion on VO_2. Values are expressed as

mean ± SD. *P < 0.05, n = 6-7 in each group. There was no significant difference in the total phase between WT and KO (p=0.08). (b) Effect of macrophage *Fth* deletion on RQ. Values are expressed as mean ± SD. **P < 0.01, n = 6-7 in each group. There was no significant difference in the light phase between WT and KO (p=0.06). (c) Effect of macrophage *Fth* deletion on energy expenditure. Values are expressed as mean ± SD. *P < 0.05, **P < 0.01, n = 6-7 in each group. There was no significant difference in the total phase between WT and KO (p=0.1). Effect of macrophage *Fth* deletion on thermogenic genes expression and body temperature in mice with HFD. (d-j) Thermogenic genes expression in epididymal fat of mice with HFD administration. Values are expressed as mean ± SD. *P < 0.05, n = 10-12 in each group. (k) Body temperature in mice with HFD administration. Values are expressed as mean ± SD. *P < 0.05, n = 12 in each group.

Fig. 8. Effect of RNA interference to H-ferritin gene on LPS-induced inflammatory cytokine expression. mRNA expression of *Fth* (a), *Fpn* (b), *Homx1* (c), and *Tfr* (d) of macrophage transfected with unrelated control siRNA or *Fth* siRNA. (e) Iron concentration with control siRNA or *Fth* siRNA transfection. Values are expressed as

mean ± SD. *P < 0.05, n = 10 in each group. (f) LPS-induced *TNF-α* mRNA expression in macrophage with unrelated control siRNA or *Fth* siRNA transfection. Values are expressed as mean ± SD. *P < 0.05, n = 4 in each group.

Table 1. Primer sequences

	Forward	Reverse
Fth	TGATGAAGCTGCAGAACCAG	GTGCAC ACTCCATTGCATTC
Ftl	AATGGGGTAAAACCCAGGAG	AG ATCCAAGAGGGCCTGATT
Hmox1	TGCTCGAATGAACACTCTGG	AAGGCGGTCTTAGCCTC
Fpn	CCCTGCTCTGGCTGTAAAAG	GGTGGGCTCTTGTTCACATT
Tfr	CCGGAGAGGAGACTTCACAG	TCCACGATTTCCCAGAGAAC
Tnf-α	ACGGCATGGATCTCAAAGAC	GTGGGTGAGGAGCACGTAGT
cpP-1	GGAGCTCATGATGTGAGCAA	GACCAGGCAAGGGAATTACA
Il-1β	CAGGCAGGCAGTATCACTCA	TGTCCTCATCCTGGAAGGTC
Il-6	CCGGAGAGGAGACTTCACAG	TCCACGATTTCCCAGAGAAC
F4/80	CTGTAACCGGATGGCAAACT	CT GTACCCACATGGCTGATG
CD11c	ATTTCTGAGAGCCCAGACGA	CCATTTGCTTCCTCCAACAT
CD68	CTTCCCACAGGCAGCACAG	AATGATGAGAGGCAGCAAGAGG
Adiponectin	GTTGCAAGCTCTCCTGTTCC	ATCCAACCTGCACAAGTTCC
Leptin	TGACACCAAAACCCTCATCA	TGAAGCCCAGGAATGAAGTC
Ucp-1	TCTCAGCCGGCTTAATGACT	TGCATTCTGACCTTCACGAC
Ucp-3	AGCCCTCTGCACTGTATGCT	AAAGGAGGGCACAAATCCTT
Adrb3	ACAGGAATGCCACTCCAATC	AAGGAGACGGAGGAGGAGAG
Ppargc1a	CCGAGAATTCATGGAGCAAT	TTTCTGTGGGTTTGGTGTGA
Dio2	GATGCTCCCAATTCCAGTGT	TGAACCAAAGTTGACCACCA
Prdm16	TGGGCTCACTACCCTACCAC	GACTTTGGCTCAGCCTTGAC
Cidea	CTCGGCTGTCTCAATGTCAA	GGAACTGTCCCGTCATCTGT
36B4	GCTCCAAGCAGATGCAGCA	CCGGATGTGAGGCAGCAG

Table 2. Red blood cell count, haemoglobin, haematocrit, mean corpuscular volume (MCV), mean corpuscular haemoglobin (MCH), and mean corpuscular haemoglobin concentration (MCHC) in each mouse.

	WT-ND	LysM-*Fth* KO-ND	WT-HFD	LysM-*Fth* KO-HFD
Red blood cell ($\times 10^4/\mu L$)	783 ± 53	767 ± 101	881 ± 69*$^{\#\#}$	901 ± 115*$^{\#\#}$
Haemoglobin (g/L)	115 ± 8	117± 4	132 ± 11**$^{\#\#}$	134 ± 17**$^{\#}$
Haematocrit (/L)	0.361 ± 0.030	0.363 ± 0.038	0.414 ± 0.035*$^{\#}$	0.412 ± 0.063*$^{\#}$
MCV (fL)	46.1 ± 2.2	47.6 ± 2.5	45.9 ± 1.6	45.5 ± 1.8
MCH (pg)	14.7 ± 0.4	15.2 ± 0.5*	15.0 ± 0.6	14.8 ± 0.4
MCHC (g/L)	318 ± 9	321 ± 9	328 ± 9	326 ± 13
Blood glucose (mmol/l)	4.2 ± 0.6	4.3 ± 0.5	6.1 ± 1.0**$^{\#\#}$	4.7 ± 0.8††
Plasma insulin (pmol/l)	18.8 ± 2.1	29.2 ± 22.2	428.5 ± 355.6**$^{\#\#}$	163.9 ± 256.3†

Data represent mean ± SD; n = 10-15; *$P < 0.05$, **$P < 0.01$ vs.WT-ND; $^{\#}P < 0.05$, $^{\#\#}P < 0.01$ vs. LysM-*Fth* KO-ND, $^{\dagger}P < 0.05$, $^{\dagger\dagger}P < 0.01$ vs. WT-HFD

Figure 1 Ikeda, et al.

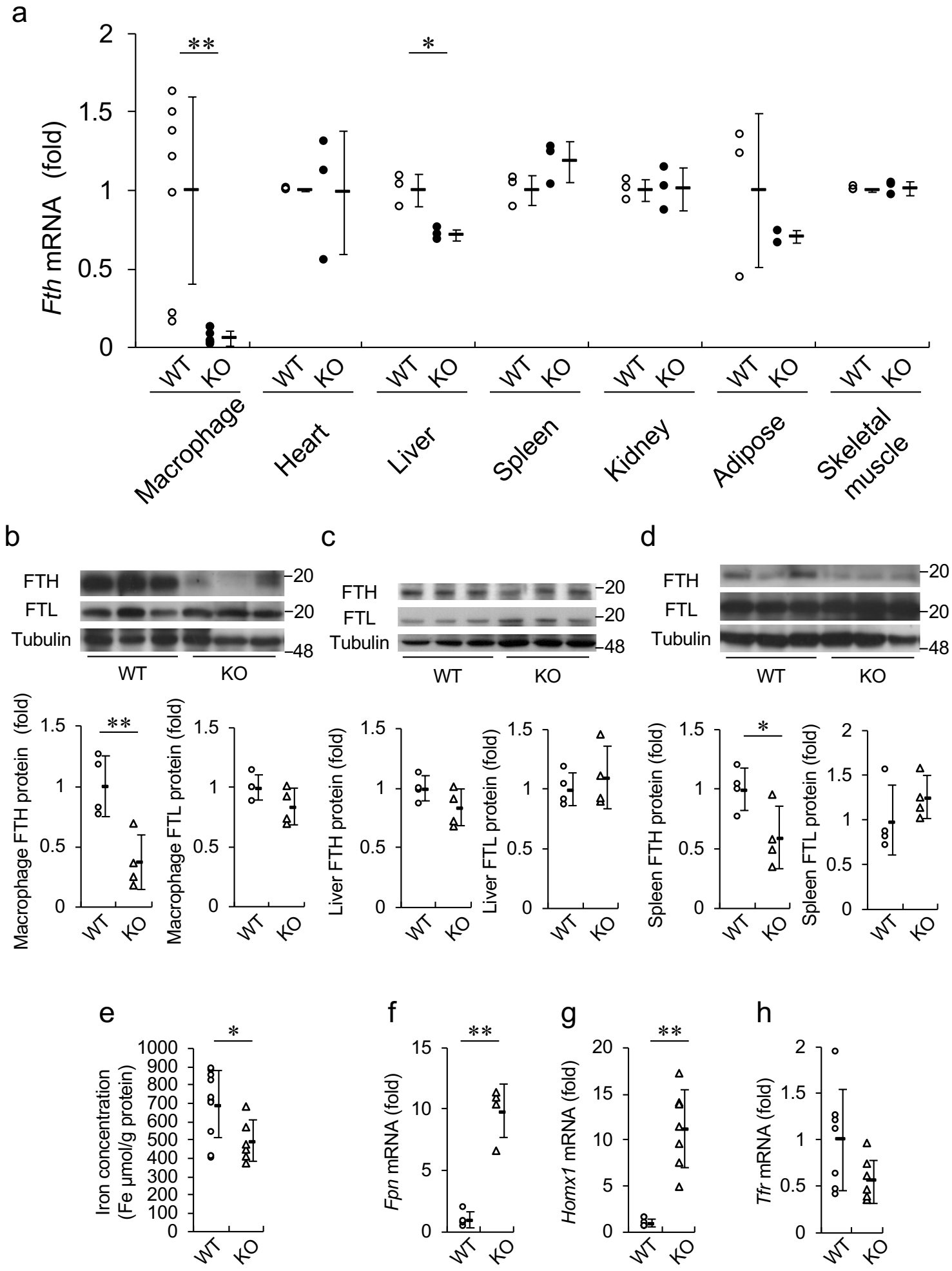

Figure 2 Ikeda, et al.

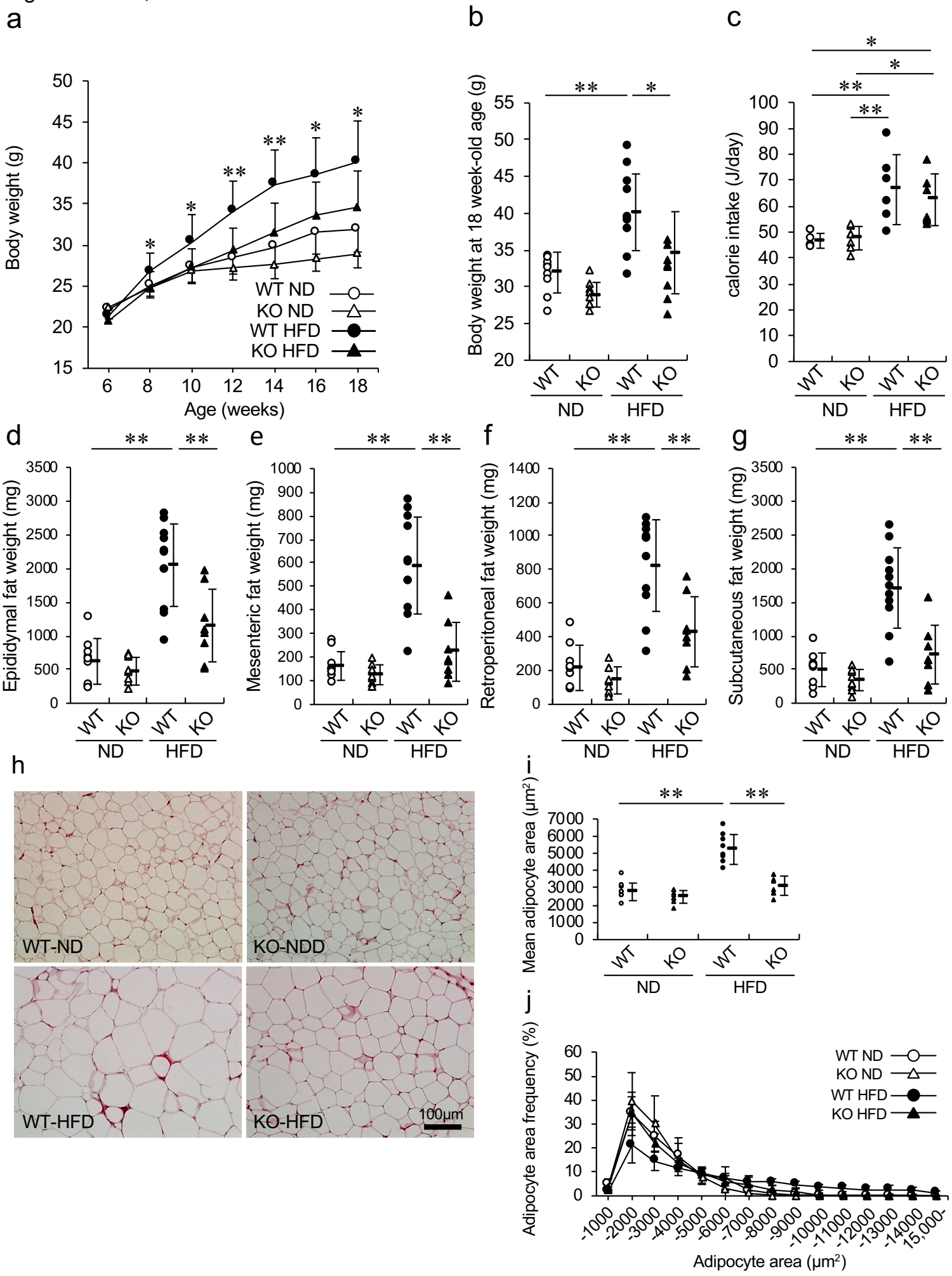

Figure 3 Ikeda, et al.

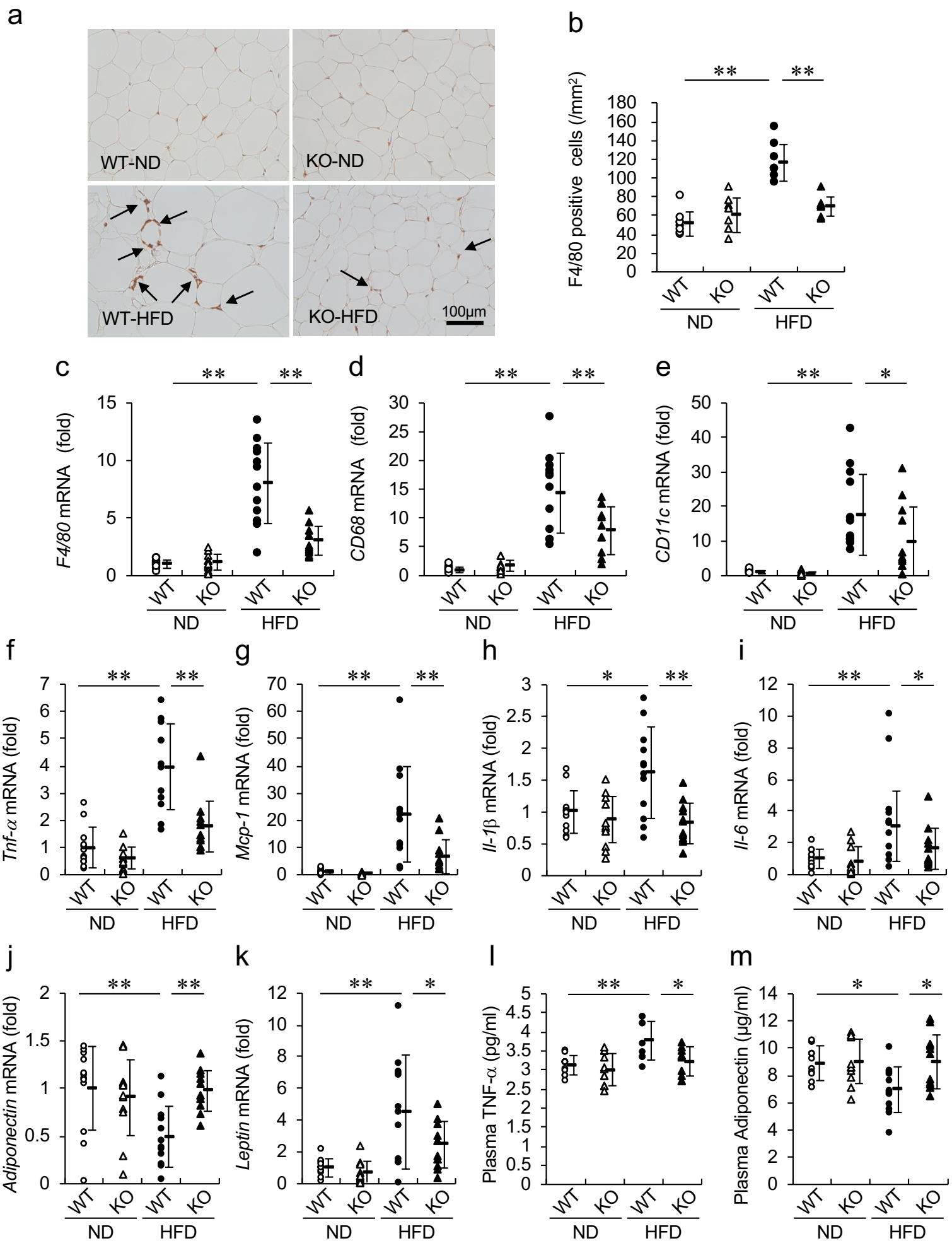

Figure 4 Ikeda, et al.

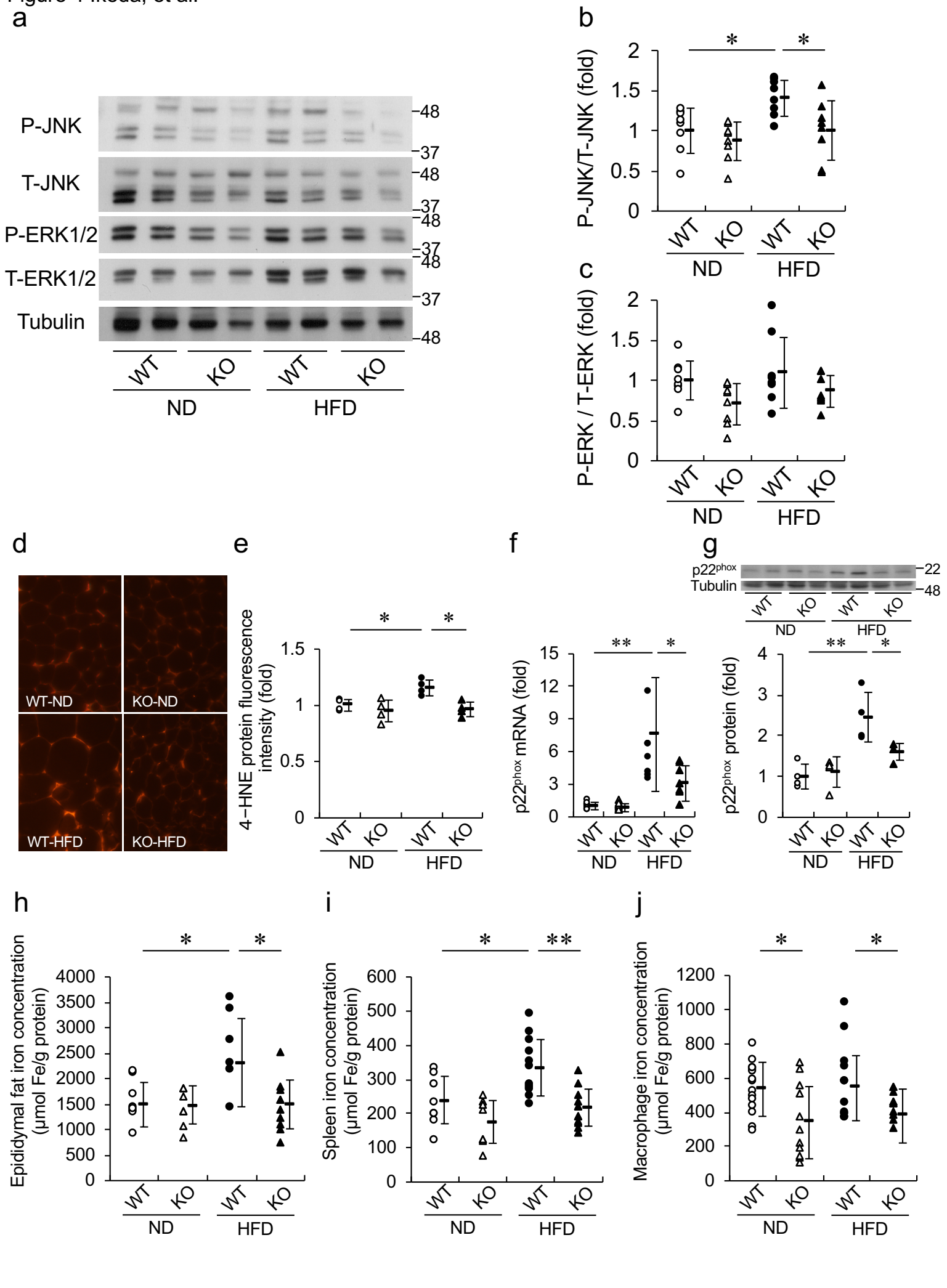

Figure 5 Ikeda, et al.

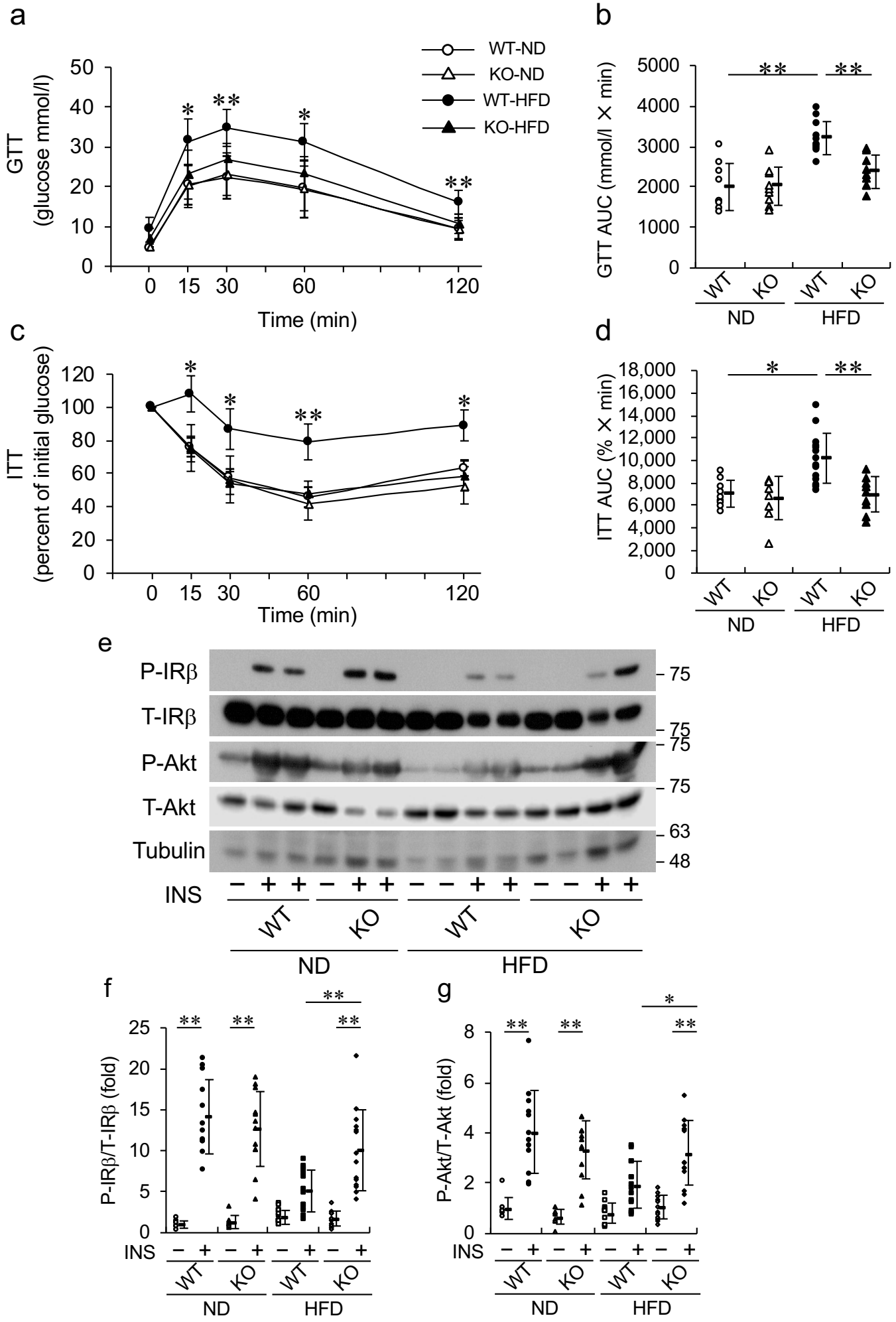

Figure 6 Ikeda, et al.

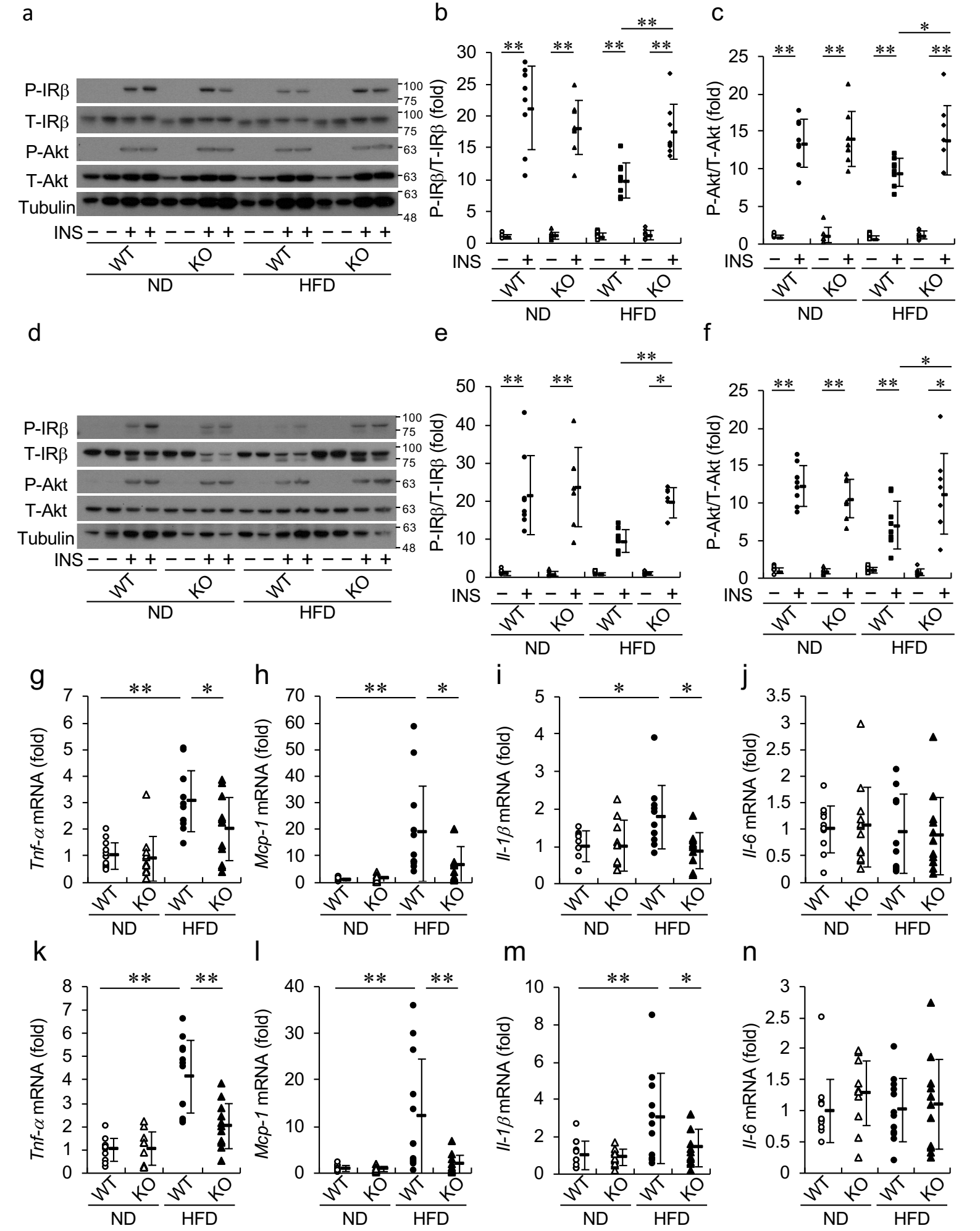

Figure 7 Ikeda, et al.

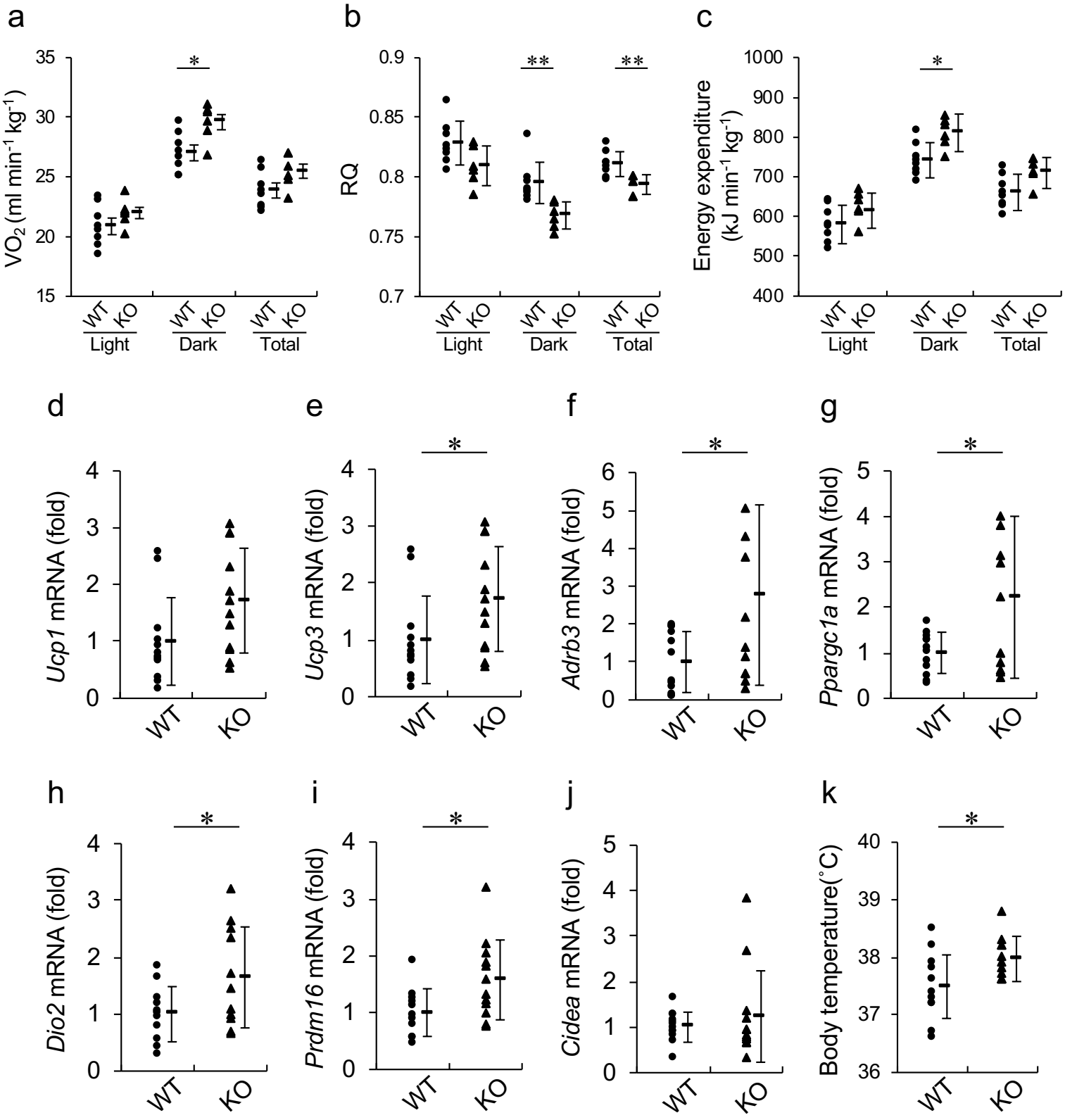

Figure 8 Ikeda, et al.